# Integrated Photonic Devices and Materials Group

**Academic and Research Staff**
Professor Leslie A. Kolodziejski, Dr. Gale S. Petrich, Principal Research Scientist

**Graduate Students**
Reginald E. Bryant, Alex J. Grine, Ryan D. Williams and Sue Y. Young

**Technical and Support Staff**
Tiffany Kuhn, Cindy Lewis-Gibbs

## Introduction

The emphasis of our research program is the design, epitaxial growth, device fabrication and characterization of a number of photonic and opto-electronic structures and devices. The epitaxial growth of the heterostructures is performed in a Veeco GEN 200 solid source, dual-reactor molecular beam epitaxy (MBE) system or in a Riber 32P gas source MBE system. The Veeco MBE system is capable of the epitaxial growth of dilute nitrides and antimony-based films in addition to arsenide- and phosphide-based films. The system platens hold multiple 2”, 3" or 4" wafers, or a single 6" or 8" wafer. The system incorporates a low wobble manipulator that will enable in-situ feedback control of the epitaxial processes using optical sensors such as band edge absorption spectroscopy and spectroscopic ellipsometry.

In the following sections, the status of the various research projects will be discussed. Projects include the development and simulation of rudimentary optical logic gates, the development and characterization of InGaAs tunnel junctions, the development of optical modulators for operation at 800nm, the development of saturable Bragg reflectors for short pulse lasers, the development of Si-based two-dimensional photonic crystal super-collimators, the development of an electrically-activated nanocavity photonic crystal laser and the development of high index contrast optical switches. These projects are collaborative efforts of multiple professors at MIT and members of the MIT Lincoln Laboratory technical staff in order to successfully design, simulate, fabricate and characterize the forementioned optical devices.

## 1. Photonic Integrated Circuits for Ultrafast Optical Logic

**Sponsors**
Defense Advanced Research Projects Agency: Contract Number: W911NF-06-1-0060

**Project Staff**
Ryan D. Williams, Dr. Aleksandra Markina, Dr. Gale S. Petrich, Professor Rajeev Ram, Professor Erich P. Ippen, Professor Leslie A. Kolodziejski, and Dr. Scott Hamilton

With an increasing demand for higher speed, switching technologies in optical telecommunications networks, there is increasing interest in both all-optical switching schemes and monolithic integration of photonic components. Reducing or eliminating optical-electronic-optical (OEO) conversions offers advantages of higher bit rates, lower power consumption, and reductions in size and weight.

The current study aims to demonstrate an optical gate consisting of semiconductor optical amplifiers (SOAs) integrated into a Mach-Zehnder interferometer on InP substrates. The optical gate offers a platform for basic Boolean functionality, wavelength conversion, and other important switching operations. Prior to fabrication, the design of the components such as the InGaAsP quaternary dilute waveguide, the multi-mode interferometers, and the adiabatic taper geometry has been optimized using beam propagation method simulations and finite-difference time-domain simulations.

To integrate the active SOA devices with the passive components, such as the multi-mode interferometers, an asymmetric twin waveguide approach is employed which eliminates the need for regrowth at the expense of additional processing steps. The first generation design consisted of two separate die: one consisting of basic isolated components and the other consisting of integrated components (Figure 1). Upon completion of processing and testing, further optimizations of the design and fabrication process were incorporated into a second generation design that is currently undergoing fabrication on campus and in collaboration with Lincoln Laboratory. In generation 2, both the active and passive devices were combined into single die suitable for a step-and-repeat mask set allowing for sharper tapers and smoother waveguide bends. Processing improvements include depositing the base metal for the top side contact prior to any III-V etching, minimizing the amount of InP-based etching through the use of trenches, and using a dedicated $CH_4/H_2$ etcher at Lincoln Laboratory. Figure 2 shows the tips of the upper active waveguide and the trench in which the passive waveguides will be centered prior to defining the passive waveguides.

In related studies, materials such as InAsP quantum dashes and InAs/InGaAs quantum dots are being explored as potential candidates for active region materials in future designs.

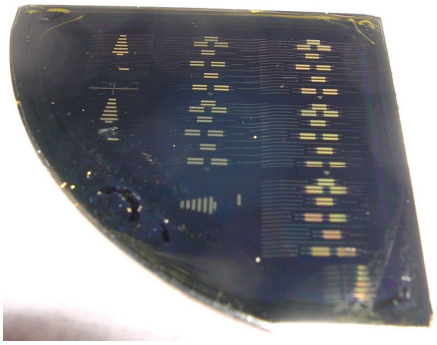

**Figure 1**. A photograph of the generation 1 fabricated dies on a quarter of a 2” InP wafer.

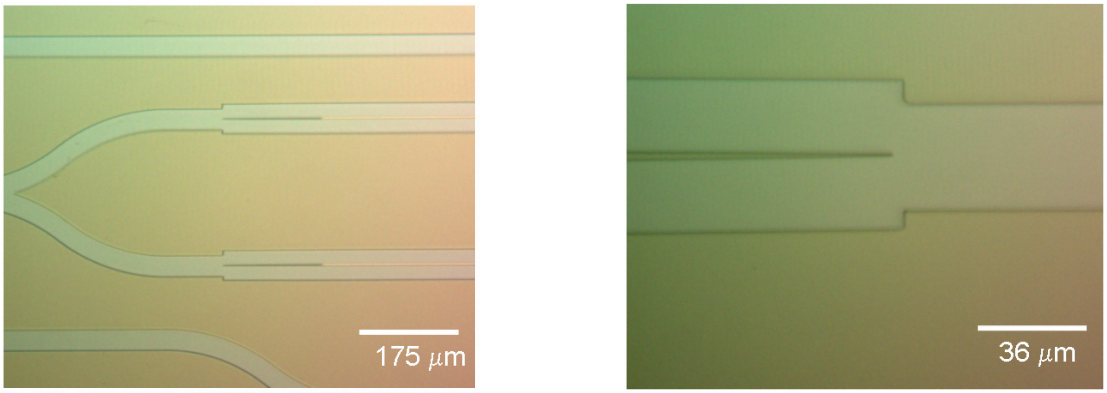


**Figure 2**. a) A photograph of the beginning of the second generation Mach Zehnder interferometer. b) A magnified view of the tip of the active waveguide prior to the definition of the lower passive waveguide.

## 2. Tunnel Junction Diodes

**Sponsors**
Defense Advanced Research Projects Agency: Contract Number: W911NF-06-1-0060

**Project Staff**
Sue Y. Young, Ryan D. Williams, Dr. Gale S. Petrich, and Professor Leslie A. Kolodziejski

The goal of this project is to characterize the tunneling behavior in InGaAs/GaAs tunnel junction diodes for use in tunnel-junction-coupled lasers. The reversed-bias leakage current of tunnel junctions can be exploited to epitaxially connect more than one lasing active region in series. Tunneling electrons from the valence band of one active region to the conduction band of a second active region can increase the external quantum efficiency of the overall device by allowing multiple photons to be emitted per injected carrier. Thus, low tunneling resistances are desired for high efficiency lasers.

The InGaAs/GaAs tunnel junction diodes were grown with varying indium contents ranging 6.5% to 13.5% while the diameter of the fabricated diode mesas ranged from 3.5 μm to 90 μm. Variable angle spectroscopic ellipsometry was performed on the epiwafers to determine the InGaAs composition and the epilayer thickness. Under both forward and reverse bias, the InGaAs tunnel junction diodes matched the theoretically predicted electrical behavior. First, the tunneling resistance decreased for increasing contact size, but, more importantly, the resistance decreased for increasing indium content (Figure 1).

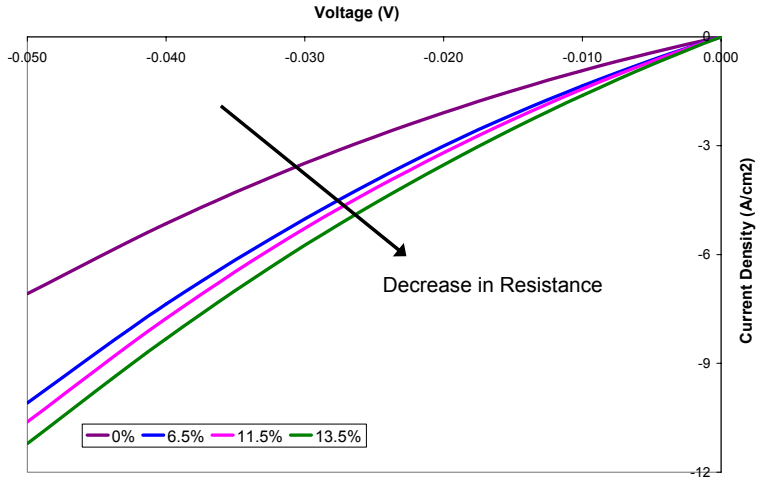


**Figure 1.** The reverse bias current density response, demonstrating a decrease in resistance for increasing indium content.

The results demonstrate that more electrons tunnel across the tunnel junction as the amount of indium is increased due to the decrease of the InGaAs bandgap. Additional tests also demonstrated that annealing the metal-semiconductor contact reduced the diode's overall resistance and that reducing the diode's temperature increased the tunnel junction resistance. With tunneling successfully demonstrated, the InGaAs tunnel junctions are implemented in GaAs-based two-stage lasers. Future work hopes to demonstrate significant increases in efficiency of tunnel-junction-coupled lasers.

### 3. Ultra Broad Band Modulator Arrays

**Sponsors**
Defense Advanced Research Projects Agency: Contract Number: W911NF-06-1-0060

**Project Staff**
Dr. Gale S. Petrich, Professor Franz X. Kaertner, Professor Erich P. Ippen and Professor Leslie A. Kolodziejski

To create an arbitrary optical waveform at wavelengths that are centered at 800nm, ultra broad band modulator arrays are required. Since these modulators are required to operate around 800nm, the material choices are limited to relatively high Al content AlGaAs and to $In_{0.5}(Ga_xAl_{1-x})_{0.5}P$ layers lattice-matched to GaAs. In addition, since GaAs absorbs light with a wavelength less than 870nm, the lower cladding layer of the modulator must be relatively thick to isolate the modulator from the GaAs substrate. To create the largest mode possible and to minimize the coupling loss, the index contrast between the waveguiding layers and the cladding layers should be minimized. To minimize the index contrast, a dilute waveguide structure in which thin layers of high index material are embedded in a low index material is employed. The resulting layered structure has an effective index slightly higher than the low index material and is determined by the layer thicknesses as well as the refractive index of the two materials that comprise the dilute waveguide. Two slightly different structures were grown by molecular beam epitaxy: (i) an InAlP-based structure in which the dilute waveguide consisted of alternating layers of InAlP and $Al_{0.5}Ga_{0.5}As$ and (ii) an $Al_{0.8}Ga_{0.2}As$-based structure in which the dilute waveguide consisted of alternating layers of $Al_{0.8}Ga_{0.2}As$ and InGaP. Both structures are challenging in terms of the epitaxial growth. In the phosphide-based structure, the growth of thick, lattice-matched InAlP cladding layers is challenging due to the need to maintain the lattice-matched condition and due to possible anion ordering. In the arsenide-based structure, although the use of $Al_{0.8}Ga_{0.2}As$ for the cladding layer minimized the lattice-mismatch problem, achieving high quality, high Al content AlGaAs cladding layers is difficult due to the low Al adatom mobility on the surface during growth. To minimize free carrier loss, p-i-n structures are employed in which the Si and Be dopant are graded from the contact layers to the dilute waveguide region. Photoluminescence measurements from the arsenide-based structure show a weak PL peak at ~650nm from the InGaP layers in the dilute waveguide. The $Al_{0.8}Ga_{0.2}As$ and $Al_{0.5}Ga_{0.5}As$ layers as well as the InAlP layers have indirect band gaps and hence do not exhibit photoluminescence. Due to the high etch selectivity between the arsenide and phosphide layers, the uppermost high index layer of the dilute waveguide also acts as an etch stop.

Both structures are anticipated to have similar optical mode profiles; the structures are designed to be single mode with a 2 micron wide ridge waveguide. Using OptiBPM, the fundamental mode for the phosphide-based structure is roughly 2 μm x 1 μm (WxH); a similar mode profile exists for the arsenide-based structure. In both structures, if the dilute waveguide is not completely etched, due to the low index contrast of the dilute waveguides, the bending radius is quite large, on the order of a millimeter.

A mask set suitable for both structures have been designed and fabricated. The mask set contains Mach Zehnder interferometer modulators of various lengths with multimode interference couplers or Y-splitters. The Mach Zehnder interferometer modulators as well as conventional modulators are oriented both parallel and perpendicular to the major flat of the 2” GaAs(100) wafers. The mask set also contains a variety of passive components such as Y-splitters, multimode interference couplers as well as straight and curved waveguides. The fabrication of the phosphide-based and arsenide-based modulators will commence shortly.

### 4. Saturable Bragg Reflectors for Modelocking Ultrafast Lasers

**Sponsor**
National Science Foundation, Award Number ECS-0322740
Office of Naval Research, Contract Number N00014-02-1-0717
Q-PEAK, PO51843
Defense Advanced Research Projects Agency: Contract Number 4R0011-05-C-0155

**Project Staff:**
Dr. Gale S. Petrich, Professor Franz X. Kaertner, Professor Erich P. Ippen and Professor Leslie A. Kolodziejski

Self-starting, modelocked, ultrafast lasers require high reflectivity mirrors with saturable absorbers. However, AlAs/GaAs or AlAs/AlGaAs mirrors with saturable absorbers exhibit a limited bandwidth due to the low index-contrast between the individual GaAs and AlGaAs layers, but are suitable for modelocking 1064 nm lasers. The reflectivity, as measured using a Varian Cary 500i spectrophotometer, and the room temperature photoluminescence are shown in Figure 1 from a saturable Bragg reflector consisting of 25 pairs of 88 nm thick $Al_{0.95}Ga_{0.05}As$ layers and 74.7nm thick GaAs layers with two 8nm thick $In_{0.27}Ga_{0.73}As$ quantum wells separated by 16nm of GaAs centered within 117nm of GaAs. The dip in the reflectivity that is due to the InGaAs quantum wells, is easily observed.

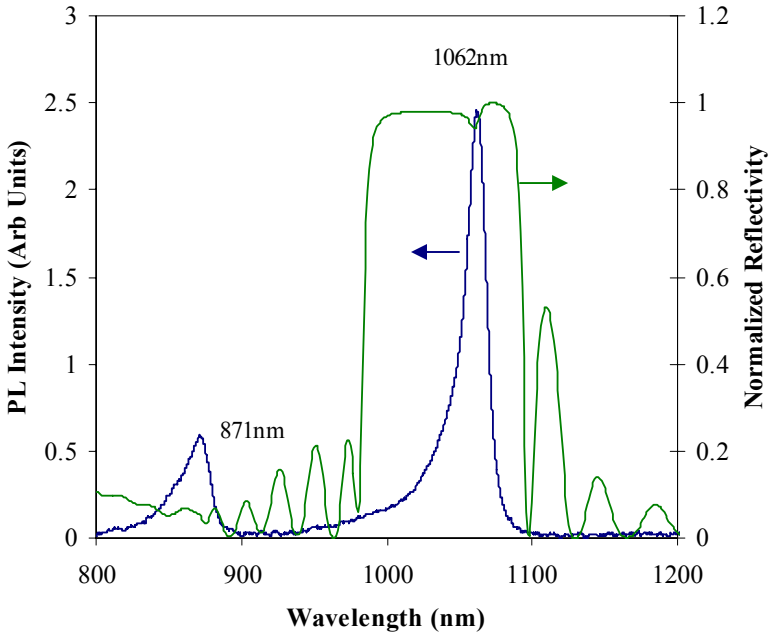


**Figure 1.** The reflectivity and photoluminescence of a InGaAs/GaAs absorber on a AlGaAs/GaAs distributed Bragg reflector.

In addition, two oxidizable saturable Bragg reflectors have been grown by molecular beam epitaxy. The SBR consists of two 8 nm InGaAs quantum wells separated by GaAs with GaAs cladding layers on a 7 pair oxidizable InGaP/AlAs dielectric stack. By thermally oxidizing the AlAs layers to form $Al_xO_y$, broadband reflectors can be created. Photoluminescence measured from the as-grown SBRs both exhibit emission at 1062 +/- 2 nm. The AlAs/InGaP mirror stacks have not been oxidized thus far.

## 5. Super-collimation of Light within Photonic Crystal Slabs

**Sponsor**
National Science Foundation, Award Number DMR-02-13282
MARCO Interconnect Focus Center, Subcontract from Georgia Institute of Technology
Contract Number B-12-M06-52

**Project Staff**
Marcus Dahlem, Peter Rakich, Dr. Sheila N. Tandon, Dr. Mihai Ibanescu, Dr. Gale S. Petrich, Prof. Marin Soljacic, Professor Erich P. Ippen, Professor John D. Joannopoulos, Professor Henry I. Smith and Professor Leslie A. Kolodziejski

A super-collimator is a device in which light is guided by the dispersion properties of a photonic crystal slab rather than by photonic crystal defects or by traditional waveguiding structures. Photonic crystals form the essence of the super-collimation effect. Being able to realize super-collimation would be potentially very useful for optical interconnects on planar lightwave circuits.

The super-collimator consists of a two-dimensional photonic crystal composed of a square lattice of cylindrical air holes etched into a high index material such as silicon. The device was fabricated using a silicon-on-insulator wafer in which the low index oxide layer (3μm thick) is used to minimize radiation loss into the high index silicon substrate. The photonic crystal occupies the entire surface of the super-collimator such that the cleaved edges of the photonic crystal function as input or output facets of the device. The initial design has focused on realizing super-collimation at a wavelength of 1500 nm such that the hole lattice constant, hole radius and Si thickness were 350nm, 105nm and 200nm, respectively.

Testing of the super-collimator device has been performed in collaboration with the Ultra-fast Optics Group. A number of characterization methods were employed to study the propagation of a 1μm diameter light beam that was launched into the silicon slab that was punctuated with the photonic crystal holes. Figure 1 shows the output of the propagating beam from a cleaved facet after traversing the photonic crystal for 5mm. In an isotropic medium, light normally spreads as it propagates. By defining the isotropic diffraction length to be the length over which the light beam spreads by root 2, super-collimation for more than 600 isotropic diffraction lengths has been observed. In Figure 1, after 5mm of propagation, the 1μm diameter incident optical beam exiting the device was found to be 2μm in size.

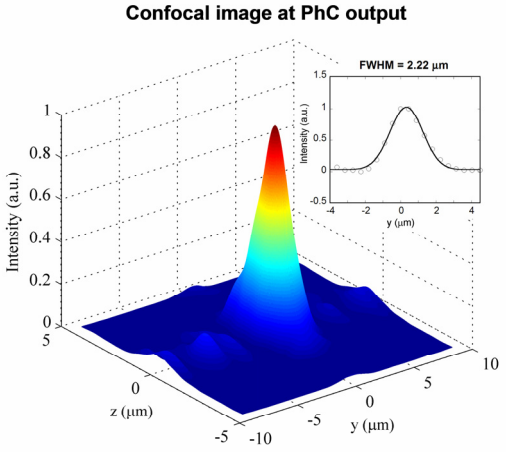


**Figure 1:** Output measured at the facet of the device for a super-collimating beam that has propagated for 5mm inside a photonic crystal silicon slab.

Using an infrared camera, images of light propagation through the photonic crystal for a number of different wavelengths could be observed from the scattered light above the sample. Figure 2a-c shows the simulated propagation of light through an ideal photonic crystal, while Figure 2d-f shows the measured scattered light as the light propagated through the super-collimator. Figure 2e shows that at a normalized frequency of ω=0.233 (λ=1510nm), light propagates through the photonic crystal in a collimated fashion as the light path resembles a stripe of light which propagates from the left to the right side of the imaging area. By tuning the wavelength of the input laser away from ω=0.233, the beam no longer exhibits a collimated behavior and begins to diverge, with the beam width expanding as it propagates the length of the imaging area. The agreement between the measured light propagation and the simulated results can be improved by including short range fabricated-related disorder (Figure 2g-i). Finally, due to the photonic crystal's dispersion surface exhibiting other "flat" regions at other frequencies, beam steering is also possible.

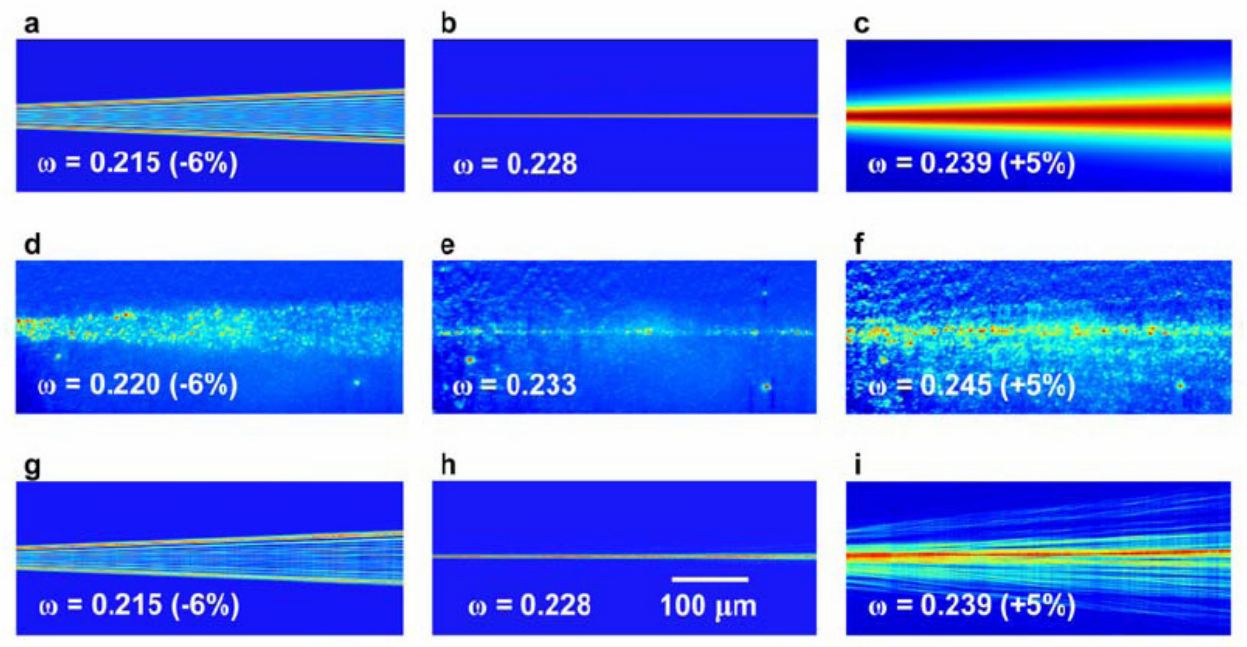


**Figure 2:** Experimental and theoretical evolution of the beam inside the photonic crystal. **a**-**c**, Theoretical beam evolution generated through beam propagation method simulations for normalized frequencies of ω = 0.239, 0.228 and 0.215, to be compared with experiment (**d**-**f**). **d**-**f**, Top-view experimental images of light traveling through the photonic crystal at wavelengths of 1430nm, 1510nm and 1610nm wavelengths that were obtained from an IR camera. Each image is approximately 500μm to the right of the point of excitation. **g**-**i**, Beam propagation method simulations of the beam evolution (for ω = 0.239, 0.228 and 0.215) including the effects of short range disorder.

## 6. Electrically-Activated Nanocavity Laser using One-Dimensional Photonic Crystals

**Sponsors**
National Science Foundation: Award Number DMR-02-13282

**Project Staff**
Alex Grine, Dr. Gale S. Petrich, and Professor Leslie A. Kolodziejski

Integrated optics provides a high speed low power option for information processing and communication. One goal of integrated optics is to extend optics' success in telecommunications, to short-range communication systems. In microprocessors, integrated optics can act as a data link between components on a single chip, or it can provide communication between chips. These applications will require some kind of optical light source, such as a laser. This project focuses on the design and fabrication of a laser well-suited as a light source for integrated optics.

This laser is particularly advantageous for use in integrated optics for several reasons: 1) The laser is electrically activated, and eliminates the need for a separate pump laser. 2) The laser only requires $25\mu m^2$ of space, which conserves chip real-estate and should lead to a relatively small threshold power. 3.) By design, the output of the laser is fed directly into a waveguide eliminating the need for separate couplers. 4.) The output is coplanar, which eases integration with other components.

The laser design (Figure 1) incorporates 1-D photonic crystals patterned on two crossing waveguides. No photonic crystals are patterned into the area where the waveguides overlap, thus creating a defect and a high Q optical resonator. In this sense, the 1-D photonic crystals act as highly reflective mirrors. By removing some of the holes one can control the direction of the emitted light. The top GaAs-based waveguide is doped p-type, while the bottom, InGaAlP-based waveguide, is doped n-type, so that a p-n diode exists only in the area where the waveguides overlap. The top GaAs waveguide contains a quantum dots-in-a-well structure which serves as the active material for the laser.

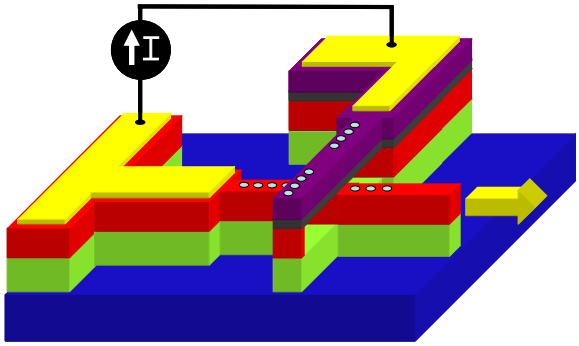


**Figure 1:** Laser schematic

A new fabrication sequence has been developed that employs either e-beam or focused ion beam lithography for sub-micron features, and photolithography for larger features allowing many lasers with varying dimensions to efficiently be processed on a single chip. A die measuring ~ ¼" x ¼" contains 280 devices each with varying features (Figure 2). This method will allow one to empirically determine the optimal device. To ease the e-beam lithography process, the mask unit cell contains an array of six devices to be processed within a 200μm field (Figure 2).

Optical simulations have led to several design changes, each with a goal of maximizing device performance, and simplifying fabrication. This has led to the inclusion of a high index InGaP core in the center of the output waveguide to confine the optical mode in the center of the output waveguide leading to more light being coupled into the output waveguide. Simulations have also revealed that a thin top waveguide reduces loss due to radiation modes. Finally, the output waveguide is tailored to be multi-mode to reduce fabrication time.

Current work includes the fabrication of the device in the Technology Research Lab, and calculations to determine figures of merit, such as output power, threshold pump power, and loss. Once fabricated, the device testing will take place in collaboration with the Ultrafast Optics and Quantum Electronics Group.

a)

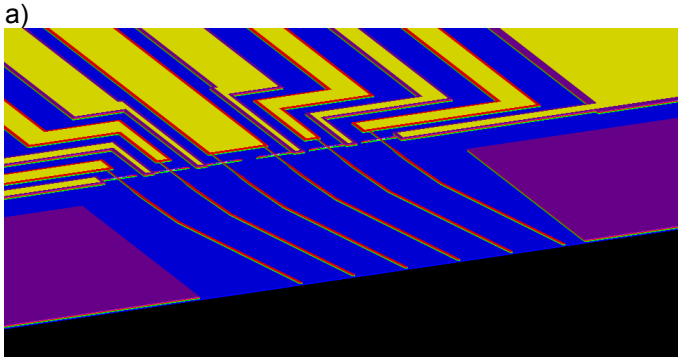

b)

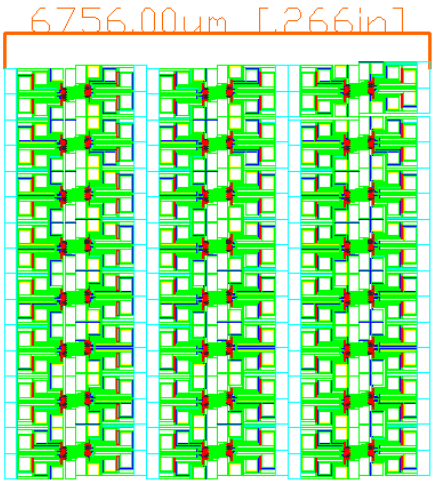


**Figure 2.** (a) Schematic of an array of 6 lasers within a 200µm field. The output waveguide is 164µm long and is angled 11˚ with respect to the facet. (b) Die measuring ~ ¼" by ¼" contains 280 different lasers. Contacts are distributed to allow easy testing.

### 7. A Nanoelectromechanically Tunable High-Index-Contrast Interference Directional Coupler

**Sponsors:**
National Science Foundation, Award Number DMR-02-13282

**Project Staff**
Reginald E. Bryant, Peter Rakich, Dr. Michelle L. Povinelli, Dr. Gale S. Petrich, Prof. Steven G. Johnson, Professor Erich P. Ippen, Professor John D. Joannopoulos, and Professor Leslie A. Kolodziejski

One of the most exciting and practical application of a directional couplers is the switch modulator where the amount of optical power coupling is adjustable. A method of tuning a single mode interference high-index-contrast (HIC) directional coupler with a nanoelectromechanical (NEM) mechanism is proposed. An electomechanically tunable directional couplers has the benefit of large changes in effective index, transparency, and low power. An HIC system has the added benefit of size reduction that allows machined nanostructures to optically guide light at a wavelength of 1.55 microns as well as to mechanically actuate.

Using GaAs waveguides with a ~300 nm square cross section, directional couplers are fabricated such that they are anchored atop of an $Al_xO_y$ as well as suspended over a trench. The anchored portions of the waveguides are adiabatically curved to a lithographically-defined coupling separation that exists suspended over the trench. The extent of which the adiabic curves are situated over the trench is determined by the desired mechanical compliance. The amount of optical power coupling is adjusted by electromechanical actuation of the waveguide separation and the S bend curvature. The selected method of electromechanical actuation utilizes a gap-closer mechanism. A gap-closer is a “spring”-suspended parallel capacitive plate mechanism that is allowed to mechanically deflect in order to reduce its capacitance. In planar MEMS/NEMS, the “spring” is usually a mechanical compliant beam (i.e. the suspended portion of the directional coupler). Gap-closers are characterized by large mechanical force densities over small displacements which makes them well suited for this particular application.

Molecular beam epitaxy is used to define layer thickness. Traditional micromachining techniques are used to lithographically define the topology and provide optical, electrical and mechanical isolation. After which, high-index-contrasting is accomplished by stream oxidation that transforms crystalline $Al_xGa_{1-x}As$ alloys of a specific composition to an amorphous $Al_xO_y$ oxide.

Nanostructure mechanical latches and bi-stable mechanisms are expected to aid in alignment accuracy. Nanostructure mechanical levers can be used to tailor the shape and angle of deflection. The device is expected to operate within the MHz regime in a speed optimized design.

## Publications

### Journal Articles, Published

P.T. Rakich, M.S. Dahlem, S. Tandon, M. Ibanescu, M. Soljacic, G.S. Petrich, J.D. Joannopoulos, L.A. Kolodziejski, E.P. Ippen, "Achieving centimetre-scale supercollimation in a large-area two-dimensional photonic crystal" *Nature Materials*, 5(2): 93-6 (2006).

F. J. Grawert, F.O. Ilay, D. Kielpinski, J.T. Gopinath, G.S. Petrich, L.A. Kolodziejski, E.P. Ippen, F.X. Kartner, "Automatic feedback control of an Er-doped fiber laser with an intracavity loss modulator" *Optics Letters*, 30(9):1066-68 (2005).

### Meeting Papers, Published

F. J. Grawert, F.O. Ilay, D. Kielpinski, J.T. Gopinath, G.S. Petrich, L.A. Kolodziejski, E.P. Ippen, F.X. Kartner, "Automatic feedback control of an Er-doped fiber laser with an intracavity loss modulator" 2005 *Conference on Lasers and Electro-Optics (CLEO)* (IEEE Cat. No. 05TH8796), 2005, pt. 3, p 1656-8 Vol. 3

### Meeting Papers, Submitted

M. Dahlem, P. Rakich, S. Tandon, M. Ibanescu, M. Soljacic, G. Petrich, J. Joannopoulos, L. Kolodziejski, E. Ippen, "Centimeter-Scale Super-Collimation in a Large-Area 2-D Photonic Crystal" *2006 Conference on Lasers and Electro-Optics (CLEO)*.

### Theses

S.Y. Young, *Characterization of Novel III-V Semiconductor Devices*, M. Eng thesis, Department of Electrical Engineering and Computer Science, MIT, 2006.

A. Markina, *Design and Simulation for the Fabrication of Integrated Semiconductor Optical Logic Gates*, Ph.D. diss., Department of Electrical Engineering and Computer Science, MIT, 2005.

S.N. Tandon, *Engineering Light using Large Area Photonic Crystal Devices,* Ph.D. diss., Department of Electrical Engineering and Computer Science, MIT, 2005.